

## Article

# Hyperspectral Estimation of Winter Wheat Leaf Water Content Based on Fractional Order Differentiation and Continuous Wavelet Transform

Changchun Li <sup>1</sup>, Zhen Xiao <sup>1,\*</sup> , Yanghua Liu <sup>2</sup>, Xiaopeng Meng <sup>1</sup>, Xinyan Li <sup>1</sup>, Xin Wang <sup>1</sup>, Yafeng Li <sup>1</sup>, Chenyi Zhao <sup>1</sup>, Lipeng Ren <sup>1</sup>, Chen Yang <sup>1</sup> and Yinghua Jiao <sup>3</sup>

<sup>1</sup> School of Surveying and Land Information Engineering, Henan Polytechnic University, Jiaozuo 454003, China

<sup>2</sup> Piesat Information Technology Co., Ltd., Beijing 100095, China

<sup>3</sup> Shandong Provincial Institute of Land Surveying and Mapping, Jinan 250102, China

\* Correspondence: xiaozhen3956@163.com

**Abstract:** Leaf water content (LWC) is one of the important indicators of crop health. It plays an important role in the physiological process of leaves, participates in almost all physiological processes of crops, and is of great significance to the survival and growth of crops. Based on the hyperspectral (350–1350 nm) and LWC data (jointing, booting, flowering, and filling periods) of winter wheat in 2020 and 2021, this work proposed to transform and process the hyperspectral data by adopting fractional order differential and continuous wavelet transform, and took a differential spectrum, wavelet coefficients, and mixed variables (differential spectrum and wavelet coefficients) as input variables of the model and adopted Gaussian process regression (GPR), classification and regression decision tree (CART), and artificial neural network (ANN) methods to estimate the LWC of wheat in different growth periods. The results indicated that fractional differential and continuous wavelet transform could highlight the spectral characteristics of winter wheat canopy and improve its correlation with LWC. The three model variables had the best estimation effect on LWC in the flowering period, and the average values of  $R^2$  were 0.86 and 0.87 in modeling and verification, which indicated that the flowering period could be used as the best estimation period for LWC. Compared with the differential spectrum and wavelet coefficients, LWC estimation based on mixed variables performed best. The average values of  $R^2$  in modeling and verification were 0.78 and 0.79. Among them, the ANN model had the highest estimation accuracy, and the  $R^2$  in modeling and verification could reach 0.92 and 0.91. This showed that fractional differential and continuous wavelet transform could effectively promote the sensitivity of spectral information to LWC and enhance the prediction ability and stability of wheat LWC. The outcomes of the present study have the potential to provide new ideas for the water monitoring of crops.

**Keywords:** winter wheat; leaf water content; fractional order differential; continuous wavelet transform; artificial neural network



**Citation:** Li, C.; Xiao, Z.; Liu, Y.; Meng, X.; Li, X.; Wang, X.; Li, Y.; Zhao, C.; Ren, L.; Yang, C.; et al. Hyperspectral Estimation of Winter Wheat Leaf Water Content Based on Fractional Order Differentiation and Continuous Wavelet Transform. *Agronomy* **2023**, *13*, 56. <https://doi.org/10.3390/agronomy13010056>

Academic Editor: Xingang Xu

Received: 17 November 2022

Revised: 15 December 2022

Accepted: 21 December 2022

Published: 23 December 2022



**Copyright:** © 2022 by the authors. Licensee MDPI, Basel, Switzerland. This article is an open access article distributed under the terms and conditions of the Creative Commons Attribution (CC BY) license (<https://creativecommons.org/licenses/by/4.0/>).

## 1. Introduction

Water is an essential component of crops, and water deficiency will affect the growth and development process and eventually affect the yield and quality. Thus, it is significant to obtain crop water content quickly and accurately for growth and development and yield improvement of crops [1,2]. In the entire tissue of crops, crop leaves have the most vigorous metabolism. Leaf water content (LWC) is an important indicator to evaluate the water status of the plant [3], and the degree of crop water deficiency can be determined by the high or low leaf water content.

Traditional LWC measurement methods are time-consuming, laborious, and inefficient, making it difficult to achieve rapid and accurate detection. In recent years, with the wide application of hyperspectral remote sensing technology in crop quality and growth

monitoring [4–8], the efficient and accurate estimation of crop LWC by hyperspectral remote sensing technology has attracted much attention from scholars. Currently, most studies construct spectral parameters based on raw spectra and then build crop LWC estimation models [9–12].

However, these methods cannot fully utilize the effective information in the spectra, thus limiting the further improvement of the accuracy of crop LWC estimation models. Fractional order differential can refine the crop detail information in the spectrum [13], which can further improve the estimation accuracy of the model. For example, Zhang Zhitao et al. [14] explored the possibility of combining the fractional order differentiation technique with the SVM-RF model to estimate the organic matter content of desert soils, and they found that the performance of the model was improved after fractional order differentiation treatment compared with integer order differentiation. Li Changchun et al. [13] used a fractional order differentiation technique to process hyperspectral data and combined it with a machine learning algorithm to establish an estimation model of winter wheat chlorophyll content. They found that the fractional order differentiation technique further improved the estimation effect of chlorophyll content. Wumuti Aishanjiang et al. [15] explored the feasibility of the fractional order differential technique and the continuous projection algorithm combined with a back-propagation neural network model to estimate wheat LWC. It was found that the fractional order differential enhanced the correlation between wheat LWC and hyperspectral data, helping to improve the estimation effect of the model.

Wavelet transform can decompose the spectral data for effective noise reduction and extract more spectral locations and feature parameters [16]. For example, Blackburn et al. [17] employed wavelet transform to decompose leaf hyperspectral data to estimate leaf chlorophyll content, and the results indicated that wavelet-based methods outperform those based on untransformed spectra and spectral parameters, and the wavelet analysis method deserves further research to quantitatively extract information from spectral data. Lin et al. [18] adopted continuous wavelet transform combined with the partial least squares method to estimate copper content in chicory leaves, which effectively improved the estimation accuracy of the copper content in chicory leaves. Tan Xianming et al. [19] used continuous wavelet transform to decompose the corn canopy spectral data. Then, an estimation model of corn canopy chlorophyll density was established, and the results indicated that compared with the vegetation target and the free combination target of bands, using wavelet coefficient to estimate chlorophyll achieved a better effect. Wang Yancang et al. [20] constructed a winter wheat LWC inversion model based on the decomposition of spectral data information by continuous wavelet transform, and the inversion effect surpassed the spectral index.

At present, the research of crop LWC estimation based on spectral data is mostly based on single variable parameters such as vegetation index, wavelet coefficient, and spectral characteristics, and few of them adopt fractional order differential and continuous wavelet transform for comprehensive comparative analysis. Therefore, this work proposed to transform and process the hyperspectral data by adopting fractional order differential and continuous wavelet transform, and GPR, CART, and ANN methods were combined to build the LWC estimation model. The objective of this study was: (i) to analyze the correlation between differential spectra and wavelet coefficient of different growth periods and LWC; (ii) based on the differential spectrum and wavelet coefficient, evaluate the ability to construct LWC estimation models for different growth periods using the GPR, CART, and ANN methods; (iii) the ability of fractional differential and continuous wavelet transform to improve the monitoring accuracy of winter wheat leaf moisture information was studied.

## 2. Materials and Methods

### 2.1. Overview of the Study Area

The experimental area is located in the Winter Wheat Comprehensive Experimental Base, Shizhuang Village, Ningguo Town, Shanyang District, Jiaozuo City, Henan. The experimental area has a warm, temperate, sub-humid monsoon climate, with sufficient sunshine, mild climate, abundant precipitation, and an annual average temperature of 14.2–14.8 °C. The soil type is Chao soil, with a pH of 7.1, organic matter content of 8.9 g/kg, total nitrogen content of 0.56 g/kg, alkali hydrolyzed nitrogen of 46.84 mg/kg, available phosphorus of 2.78 mg/kg, and available potassium of 112.00 mg/kg. Two wheat varieties, Jing 9843 and Zhong Mai 175, were set up in the study area, with four fertilizer gradients (0, 195, 390, and 585 kg/ha). Three water treatments were set, namely: rainfed (no irrigation), normal water (irrigation water volume is 192 mm), and twice normal water (irrigation water volume is 384 mm). There were three treatments, 16 plots per treatment, and 48 plots in total. The size of each plot is 8 m × 6 m. The field management conditions of each plot were the same, and the geographical location of the study area is shown in Figure 1.

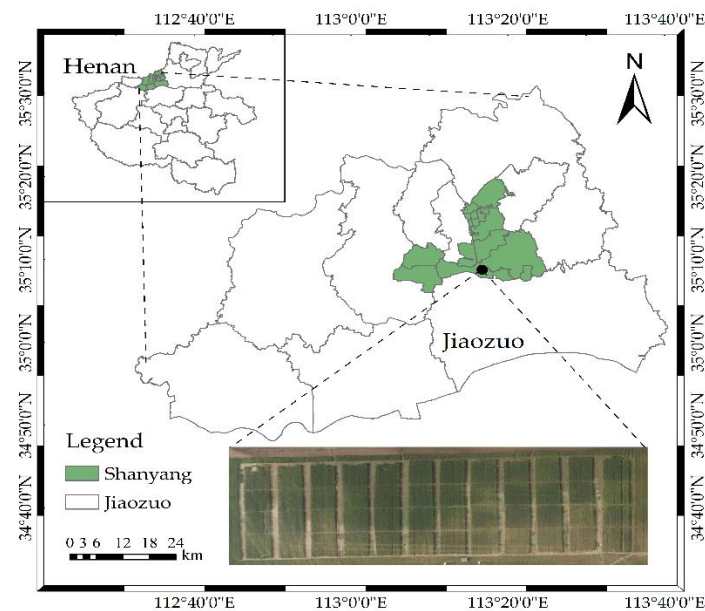


**Figure 1.** The schematic of the study area.

### 2.2. Data Collection and Processing

The hyperspectral reflectance and LWC data of the wheat canopy were obtained in 48 plots in 2020 and 2021 separately, and the data of four key growth periods, namely, the jointing period, booting period, flowering period, and filling period, were collected.

#### 2.2.1. Hyperspectral Data Collection and Processing

The American ASD Field Spec ®4 Hi-Res (Analytica Spectra Devices, Inc., Langmont, CO, USA) spectrometer was used to collect wheat canopy hyperspectral data. The wavelength range of the instrument was 350–2500 nm, and the resampling interval was 1 nm. The sampling interval included 1.4 nm (350–1000 nm) and 2 nm (1001–2500 nm). The specific time for data collection in clear and windless weather was from 10:30 to 14:30. The spectral data collected in this time period were more stable than those collected in other time periods. When collecting data, the probe was vertically downward with a field angle of 25°, which was 30 to 40 cm above the winter wheat canopy to reduce the impact of the soil background. Moreover, to eliminate the impact of external light changes on spectral data acquisition, the BaSO<sub>4</sub> whiteboard calibration was performed every 10–20 min. Each plot randomly selected three sample points that could represent the overall growth of wheat. For each sample point, 10 spectral curves were collected, and the average reflectance of the

three sample points was regarded as the spectral reflectance value of the plot. After data acquisition, the spectral data were preprocessed by the Savitzky–Golay filtering method. Moreover, to eliminate the influence of noise in the spectral data, hyperspectral reflectance data in the range of 350–1350 nm were selected for analysis and modeling.

### 2.2.2. LWC Data Measurement

The LWC of wheat was obtained by the drying method. Five representative samples of wheat leaves were randomly selected from each plot, and 20 fully expanded leaves were collected from the upper part of the wheat canopy, and the average LWC value of the 100 leaves was regarded as the LWC value of the plot. The collected leaves were sealed, and the fresh weight of the leaf samples was weighed by precision electronic scales (0.001 g) in the laboratory. Then, they were put into the oven (80 °C) and dried to constant weight, and the dry weight of the leaf samples was weighed; finally, the LWC was calculated using Equation (1):

$$\text{LWC} = \frac{\text{FW} - \text{DW}}{\text{FW}} \times 100\% \quad (1)$$

where FW represents the fresh weight of the leaf sample, and DW represents the dry weight of the leaf sample.

## 2.3. Data Processing Methods

### 2.3.1. Fractional Order Differentiation

Fractional order differentiation is a further development of integer differentiation. It may decompose spectral data, deeply mine sensitive information, and is widely used in agricultural remote sensing [21,22]. There are three brands of fractional differentiation. In this work, because the definition form of Grünwald–Letnikov is simple and understandable, it is used to transform and decompose hyperspectral data [23]. The expression is as follows:

$$\frac{d^\alpha f(\lambda)}{d\lambda^\alpha} = f(\lambda) + (-\alpha)f(\lambda - 1) + \frac{(-\alpha)(-\alpha + 1)}{2} + \dots + \frac{\Gamma(-\alpha + 1)}{n!(-\alpha + 1)}f(\lambda - n) \quad (2)$$

where  $\alpha$  is the order,  $\lambda$  is the spectral wavelength,  $\Gamma$  is the Gamma function, and  $n$  is the D-value of the bound limits of the differential equation.

### 2.3.2. Continuous Wavelet Transform

Continuous wavelet transform performs local refinement analysis of a signal based on time and spatial frequency, which can decompose a complex signal into a series of wavelet coefficients of different scales [24]. In this work, the continuous wavelet transform is employed to decompose the spectral data. As a mathematically linear transformation method often used to process hyperspectral data [25–27], the continuous wavelet transform can better process and interpret spectral information. The calculation is shown in Equations (3) and (4):

$$W_f(a, b) = \int_{-\infty}^{+\infty} f(\lambda)\psi_{a,b}(\lambda)d\lambda \quad (3)$$

$$\psi_{a,b}(\lambda) = \frac{1}{\sqrt{a}} \left( \frac{\lambda - b}{a} \right) \quad (4)$$

where  $\lambda$  is the spectral wavelength,  $a$  is the scale factor,  $b$  is the translation factor,  $f(\lambda)$  represents the hyperspectral reflectance, and  $\psi_{a,b}$  represents the wavelet basis.

## 2.4. Modeling Methods

### 2.4.1. Gaussian Process Regression

Gaussian process regression (GPR) is a machine learning method that uses a GP prior to regression modeling with properties determined by the mean and covariance [28]. GP is a collection of random variables all obeying joint gaussian distribution, which is essentially a multivariate gaussian distribution [29]. GPR ensures that the prediction error falls within

a certain range for the training data, and it can adjust the complexity of the model. Thus, it is suitable for dealing with nonlinear regression, small samples, high dimensionality, etc.

#### 2.4.2. Classification and Regression Tree

A decision tree is a method based on classification and regression. When it is used in regression analysis, it usually refers to the classification and regression tree (CART) [30]. The principle of regression trees is to divide the feature plane into several cells, with each division corresponding to a specific output. The model has a fast training speed and is good at obtaining nonlinear relationships in the dataset.

#### 2.4.3. Artificial Neural Network

The artificial neural network (ANN) was proposed by Rumelhart and McClelland in 1986 [31]. It is a multilayer feedforward neural network with backward propagation of errors, mimicking the human brain nervous system in processing complex information, so it has powerful self-learning and self-adaptive capabilities. ANN mainly contains an input layer, a hidden layer, and an output layer. The model variables are input by the input layer; then, the input attribute information is sent to the hidden layer by using the Sigmoid function; finally, the target data are output after the processing of the hidden layer. If the error between the target data and the actual data exceeds the set threshold, the error information is fed back to the hidden layer, and the data processing is continued until the error satisfies the requirement. Specifically, the model variables of the input layer include 10 fractional differential spectra, 10 wavelet energy coefficients, and mixed variables selected, and the output data of the output layer are LWC estimation data.

In each growth period, the data sets were divided at a ratio of 3:1, where 36 specimens were chosen to build the modeling dataset, and 12 specimens were chosen to build the validation dataset. The differential spectra and wavelet energy coefficients were used as independent variables with LWC as the dependent variable to build the winter wheat LWC estimation model. Each model regression framework was constructed and implemented in R language v4.0.2.

#### 2.5. Correlation Analysis

The Pearson correlation coefficient ( $\rho$ ) was adopted for correlation analysis. The value of the correlation coefficient is between  $-1$  and  $1$ ; the larger the absolute value, the greater the correlation between the two variables; conversely, the closer the value is to  $0$ , the lower the correlation between the two variables [32].

#### 2.6. Model Performance Evaluation

The coefficient of determination ( $R^2$ ), root mean squared error (RMSE), and standard root mean squared error (nRMSE) are chosen as the precision evaluation metrics of the model [33,34].

### 3. Results

#### 3.1. Statistical Characteristics of LWC in Wheat

The main statistical characteristics of wheat LWC in each period of different years are shown in Table 1. It can be seen from Table 1 that in 2020, the LWC change range at the jointing period was 71.04–79.89%, at the booting period was 71.85–79.48%, at the flowering period was 68.94–78.44%, and at the filling period was 29.85–71.80%. In 2021, the change range of LWC at the jointing period was 72.97–81.87%, at the booting period was 73.86–82.20%, at the flowering period was 60.53–75.27%, and at the filling period was 46.09–67.97%. On the whole, the average value of LWC in different years showed a trend of first increasing and then decreasing with the advance of the growth period. The average value of LWC in the booting period reached the maximum, and that in the filling period reached the minimum. In addition, the SD of LWC in different years increased gradually with the advance of fertility.

**Table 1.** Statistical characteristics of LWC from each growth period in different years.

Growth Periods	LWC (%)							
	2020				2021			
	MAX	MIN	MEAN	SD	MAX	MIN	MEAN	SD
Jointing period	79.89	71.04	76.19	1.70	81.87	72.97	77.11	2.05
Booting period	79.48	71.85	76.42	1.80	82.20	73.86	78.71	2.06
Flowering period	78.44	68.94	73.40	2.35	75.27	60.53	67.43	3.94
Filling period	71.80	29.85	61.38	9.26	67.97	46.09	60.39	5.21

MAX means maximum value; MIN means minimum value; SD means standard deviation.

### 3.2. Estimation of Wheat LWC Based on Fractional Order Differential

#### 3.2.1. Analysis of Correlation between Original Hyperspectral and Fractional Order Differential Spectrum and LWC

The original hyperspectral data of four growth periods of winter wheat were processed by using the Grünwald–Letnikov form of the fractional differential method, where the order range was 0–2 and the step size was set to 0.1. The original spectra and differential spectra in the four periods were analyzed for correlation with the LWC, and the correlation coefficient is shown in Figures 2 and 3 (where red represents positive correlation, blue represents negative correlation, and the darker the same color is, the stronger the correlation between the spectral variables and the LWC). Meanwhile, 10 differential spectra with greater correlation with LWC were chosen, and their relevance matrix with LWC is presented in Figure 4.

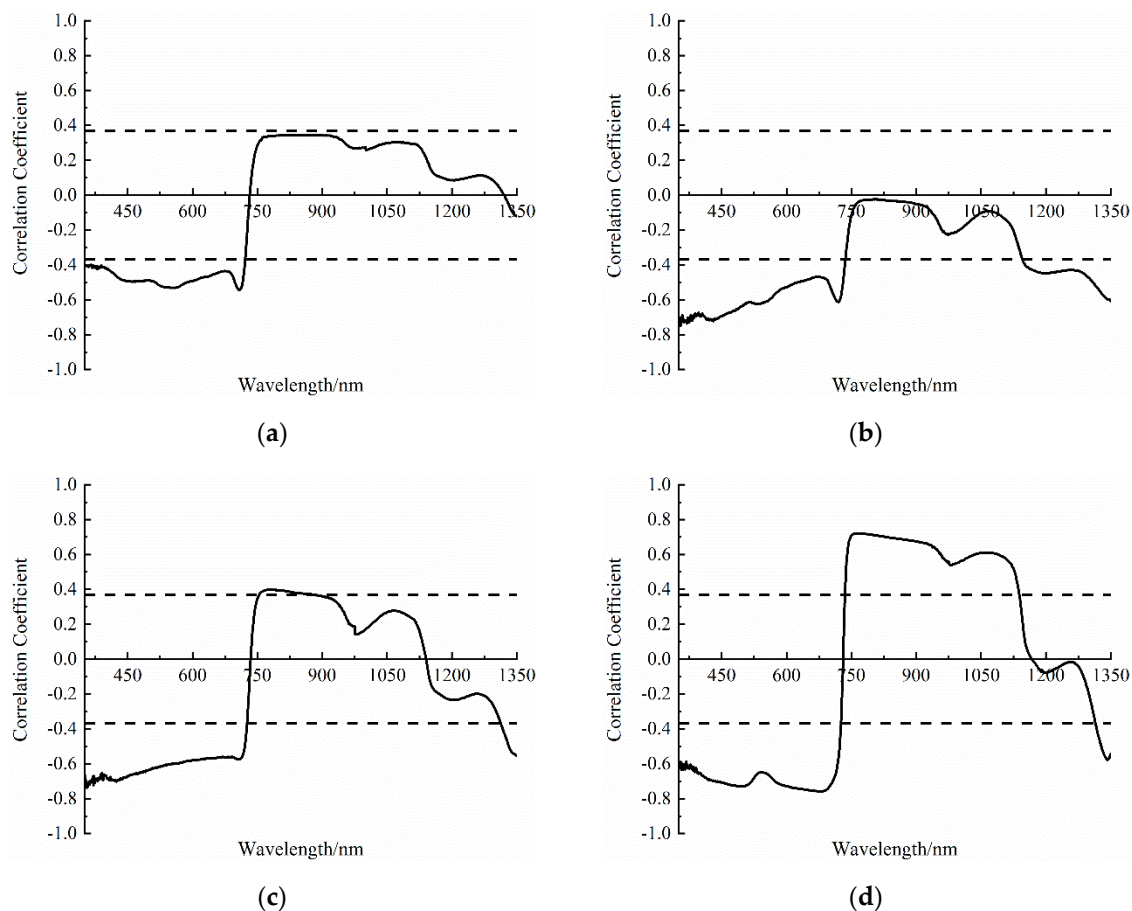


**Figure 2.** Correlation analysis of the raw hyperspectral with LWC in four growth periods. (a) Jointing period; (b) booting period; (c) flowering period; (d) filling period.

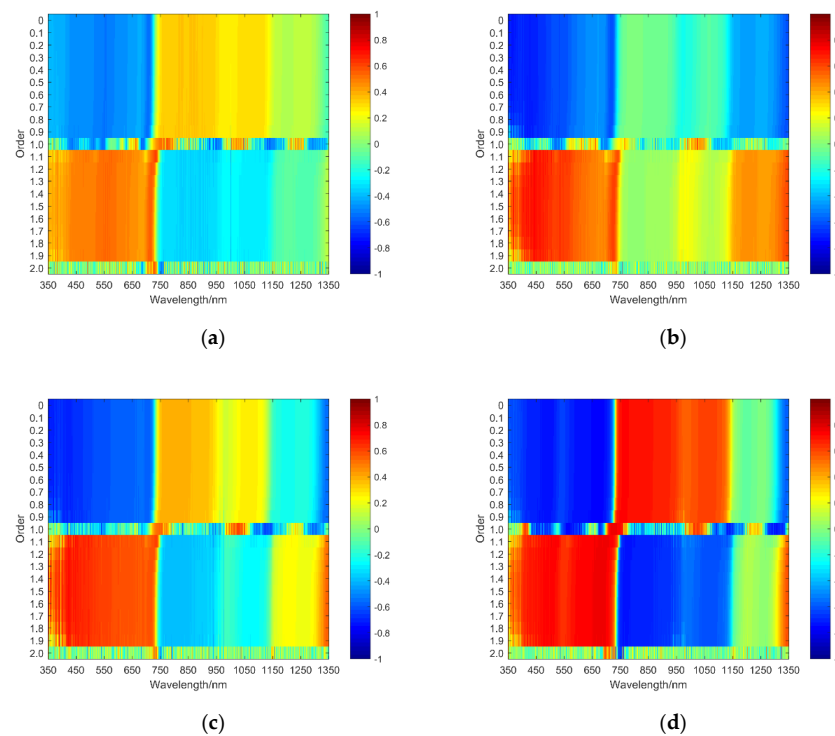


**Figure 3.** The relevance between the spectra of different growth periods and LWC. (a) Jointing period; (b) booting period; (c) flowering period; (d) filling period.

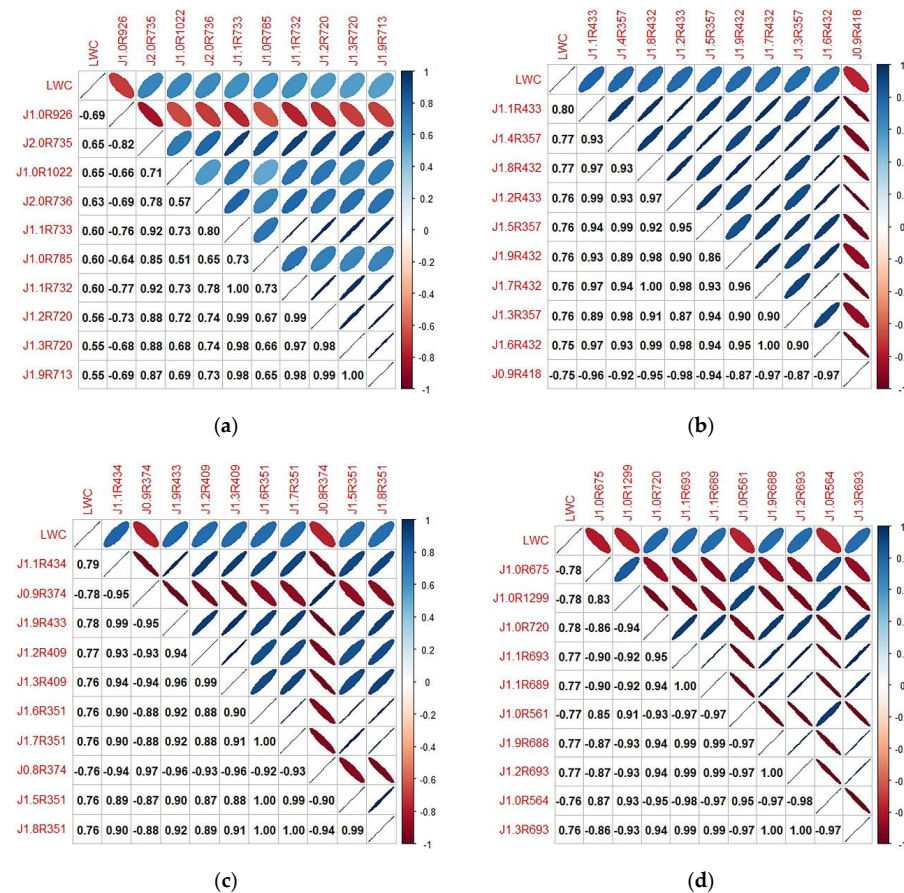


**Figure 4.** The relevance matrix of the selected fractional order differential spectra with LWC in four growth periods. (a) Jointing period; (b) booting period; (c) flowering period; (d) filling period.

The following observations can be obtained from the analysis of Figures 2–4:

1. In the jointing period, the correlation between the original hyperspectral data and the LWC was analyzed. It could be seen from Figure 2a that there was a significant negative correlation with the LWC at a level of 0.01 within the wavelength from 350 to 721 nm. When the negative correlation was the strongest, the wavelength was 708 nm, and the correlation coefficient  $\rho$  was  $-0.54$ . The correlation between the differential spectrum and the LWC was analyzed. It could be seen from Figure 3a that the absolute value of the  $|\rho|$  of each order of the differential spectrum and LWC was greater than 0.54. When the order was 1.0, the  $|\rho|$  reached a maximum of 0.69 at a wavelength of 926 nm. Except for orders 1.0 and 2.0, more than 347 differential spectral bands reached a significant level of 0.01. At the jointing period, 10 differential spectra were selected as follows: J1.0R926, J2.0R735, J1.0R1022, J2.0R736, J1.1R733, J1.0R785, J1.1R732, J1.2R720, J1.3R720, and J1.9R713, respectively. The correlation results were shown in Figure 4a.
2. In the booting period, the correlation between the original hyperspectral data and the LWC was analyzed. It could be seen from Figure 2b that there was a significant negative correlation with the LWC at a level of 0.01 within the wavelength from 353 to 735 nm and 1149 to 1350 nm. The negative correlation was the strongest at 355 nm, and the  $\rho$  value was  $-0.75$ . Then, the correlation between the differential spectrum and the LWC was analyzed. It could be seen from Figure 3b that the  $|\rho|$  value of each order of the differential spectrum and LWC were greater than 0.73. When the order was 1.1, the wavelength was at 433 nm, and the  $|\rho|$  value was up to a maximum of 0.80. Except for order 1.0 and order 2.0, more than 558 differential spectral bands reached a significance level of 0.01. At the booting period, 10 differential spectra were selected as follows: J1.1R433, J1.4R357, J1.8R432, J1.2R433, J1.5R357, J1.9R432, J1.7R432, J1.3R357, J1.6R432, and J0.9R418, respectively. The correlation results are shown in Figure 4b.
3. In the flowering period, the correlation between the primitive hyperspectral data and the LWC was analyzed. According to Figure 2c, there was a significant negative correlation with the LWC at a level of 0.01 at wavelengths from 350 to 725 nm and 1316 to 1350 nm, and a significant positive correlation with the LWC at a level of 0.01 from 760 to 828 nm. When the correlation was strongest, the wavelength was 356 nm, and the  $\rho$  value was  $-0.74$ . Then, the correlation between the differential spectrum and the LWC was analyzed. According to Figure 3c, the  $|\rho|$  value of each order of the differential spectrum and LWC was greater than 0.72. When the order was 1.1, the  $|\rho|$  value was up to a maximum of 0.79 at a wavelength of 434 nm. Except for orders 1.0 and 2.0, more than 518 differential spectral bands reached a significance level of 0.01. At the jointing period, 10 differential spectra were selected as follows: J1.1R434, J0.9R374, J1.9R433, J1.2R409, J1.3R409, J1.6R351, J1.7R351, J0.8R374, J1.5R351, and J1.8R351, respectively. The correlation results are shown in Figure 4c.
4. In the filling period, the correlation between the primitive hyperspectral data and the LWC was analyzed. It could be seen from Figure 2d that there was a significant negative correlation with the LWC at a level of 0.01 at wavelengths from 350 to 725 nm and 1316 to 1350 nm, and a significant positive correlation with the LWC at a level of 0.01 from 736 to 1137 nm; the strongest correlation was obtained at 680 nm, with the  $\rho$  value of  $-0.76$ . Then, the correlation between the differential spectrum and the LWC was analyzed. As shown in Figure 3d, the maximum value of  $|\rho|$  was greater than 0.72. When the order was 1, the  $|\rho|$  value reached a maximum of 0.78 at a wavelength of 675 nm. Except for orders 1.0 and 2.0, more than 792 differential spectral bands achieved a significant level of 0.01. At the jointing period, 10 differential spectra were selected as follows: J1.0R675, J1.0R1299, J1.0R720, J1.1R693, J1.1R689, J1.0R561, J1.9R688, J1.2R693, J1.0R564, and J1.3R693, respectively. The correlation results are shown in Figure 4d.

### 3.2.2. Construction and Analysis of LWC Estimation Model

In each growth period, the 10 fractional differential spectrums screened were taken as independent variables and LWC as dependent variables. Then, 75% of the specimen data were randomly selected, and three methods, namely GPR, CART, and ANN, were used to estimate LWC for different growth periods of wheat. The remaining 25% of the specimen data were used for model accuracy verification. The results are presented in Table 2.

**Table 2.** The LWC estimation results obtained by adopting differential spectra combined with GPR, CART, and ANN for different growth periods.

Growth Periods	Method	Modeling Accuracy			Verification Accuracy		
		R <sup>2</sup>	RMSE (%)	nRMSE (%)	R <sup>2</sup>	RMSE (%)	nRMSE (%)
Jointing period	GPR	0.72 **	1.05	1.38	0.75 **	0.97	1.26
	CART	0.61 **	1.07	1.40	0.62 **	1.27	1.68
	ANN	0.61 **	1.06	1.39	0.69 **	0.98	1.28
Booting period	GPR	0.79 **	0.91	1.19	0.84 **	0.83	1.08
	CART	0.74 **	0.94	1.22	0.76 **	1.13	1.50
	ANN	0.71 **	1.00	1.31	0.69 **	1.02	1.35
Flowering period	GPR	0.87 **	1.03	1.40	0.85 **	1.24	1.68
	CART	0.78 **	1.08	1.47	0.86 **	1.51	2.03
	ANN	0.89 **	0.80	1.09	0.88 **	1.14	1.56
Filling period	GPR	0.85 **	4.36	7.02	0.78 **	5.34	8.63
	CART	0.72 **	5.14	8.38	0.81 **	4.38	6.82
	ANN	0.85 **	3.82	6.25	0.83 **	2.89	4.61

\*\* indicates  $p \leq 0.01$ .

The following observations can be obtained from Table 2:

1. In the jointing period, the modeling accuracy of the GPR model was  $R^2 = 0.72$ ,  $RMSE = 1.05\%$ , and  $nRMSE = 1.38\%$ , and the validation accuracy was  $R^2 = 0.75$ ,  $RMSE = 0.97\%$ , and  $nRMSE = 1.26\%$ . Compared with the CART model and the ANN model, the modeling and validation  $R^2$  of the GPR increased by 0.11 and 0.13, and 0.11 and 0.06, the RMSE decreased by 0.02% and 0.30%, and 0.01% and 0.01%, and the nRMSE decreased by 0.02% and 0.42%, and 0.01% and 0.02%, respectively. The GPR model achieved higher modeling and verification accuracy than the other two models. A comprehensive analysis indicated that the GPR model had a better estimation effect in the jointing period.
2. In the booting period, the modeling accuracy of the GPR model was  $R^2 = 0.79$ ,  $RMSE = 0.91\%$ , and  $nRMSE = 1.19\%$ , and the validation accuracy was  $R^2 = 0.84$ ,  $RMSE = 0.83\%$ , and  $nRMSE = 1.08\%$ . Compared with the CART model and the ANN model, the modeling and validation  $R^2$  of the GPR increased by 0.05 and 0.08, and 0.08 and 0.15, the RMSE decreased by 0.03% and 0.30%, and 0.09 and 0.19%, and the nRMSE decreased by 0.03% and 0.42%, and 0.12% and 0.27%, respectively. The GPR model achieved higher modeling and verification accuracy than the other two models. Through a comprehensive analysis, it was shown that the GPR model had a better estimation effect in the booting period.
3. In the flowering period, the modeling accuracy of the ANN model was  $R^2 = 0.89$ ,  $RMSE = 0.80\%$ , and  $nRMSE = 1.09\%$ , and the validation accuracy was  $R^2 = 0.88$ ,  $RMSE = 1.14\%$ , and  $nRMSE = 1.56\%$ . Compared with the GPR model and the CART model, the modeling and validation  $R^2$  of the ANN increased by 0.02 and 0.03, and 0.11 and 0.02, and the RMSE decreased by 0.23% and 0.10%, and 0.28% and 0.37%, and the nRMSE decreased by 0.31% and 0.12%, and 0.38% and 0.47%, respectively. The ANN model achieved higher modeling and verification accuracy than the other two models. Through a comprehensive analysis, it was found that the ANN model had the highest estimation accuracy in the flowering period.

4. In the filling period, the modeling accuracy of the ANN model was  $R^2 = 0.85$ , RMSE = 3.82%, and nRMSE = 6.25%, and the validation accuracy was  $R^2 = 0.83$ , RMSE = 2.89%, and nRMSE = 4.61%. Compared with the GPR model and the CART model, the modeling and validation  $R^2$  of the ANN increased by 0.00 and 0.05, and 0.13 and 0.02, and the RMSE decreased by 0.54% and 2.45%, and 1.32% and 1.49%, and the nRMSE decreased by 0.77% and 4.02%, and 2.13% and 2.21%, respectively. The ANN model achieved higher modeling and verification accuracy than the other two models. A comprehensive analysis indicated that the ANN model had a better estimation effect in the filling period.

When fractional order differential spectroscopy was combined with GPR, CART, and ANN to estimate LWC in different growth periods, the GPR achieved good estimation results in the jointing and panicle periods, and the ANN model had the highest estimation accuracy in the flowering and filling periods.

### 3.3. Estimation of Wheat LWC Based on Continuous Wavelet Transform

#### 3.3.1. Correlation Analysis between Wavelet Coefficients and LWC

The original hyperspectral data of the four growth periods were decomposed at different scales through continuous wavelet transform to obtain wavelet coefficients at the decomposition scale from 1 to 10, in which the wavelet base was Mexican Hat, the second derivative of the Gaussian function. Then, the correlation between the wavelet coefficient and the LWC in the four periods was analyzed, and the correlation between the wavelet coefficient and the LWC in each growth period was obtained. The results are shown in Figure 5. Meanwhile, 10 wavelet coefficients with greater correlation were chosen to draw their correlation matrix with LWC, and the results are illustrated in Figure 6.

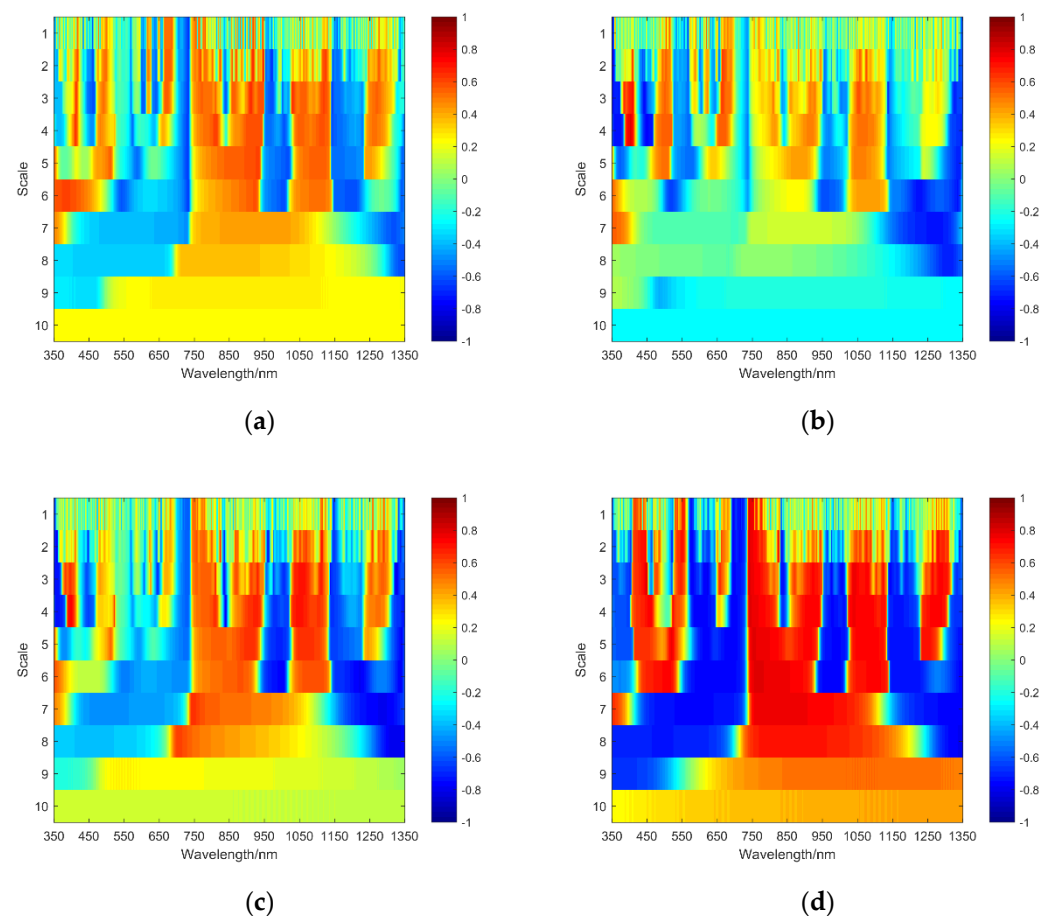


**Figure 5.** The relevance between the wavelet coefficient of different growth periods and LWC. (a) Jointing period; (b) booting period; (c) flowering period; (d) filling period.

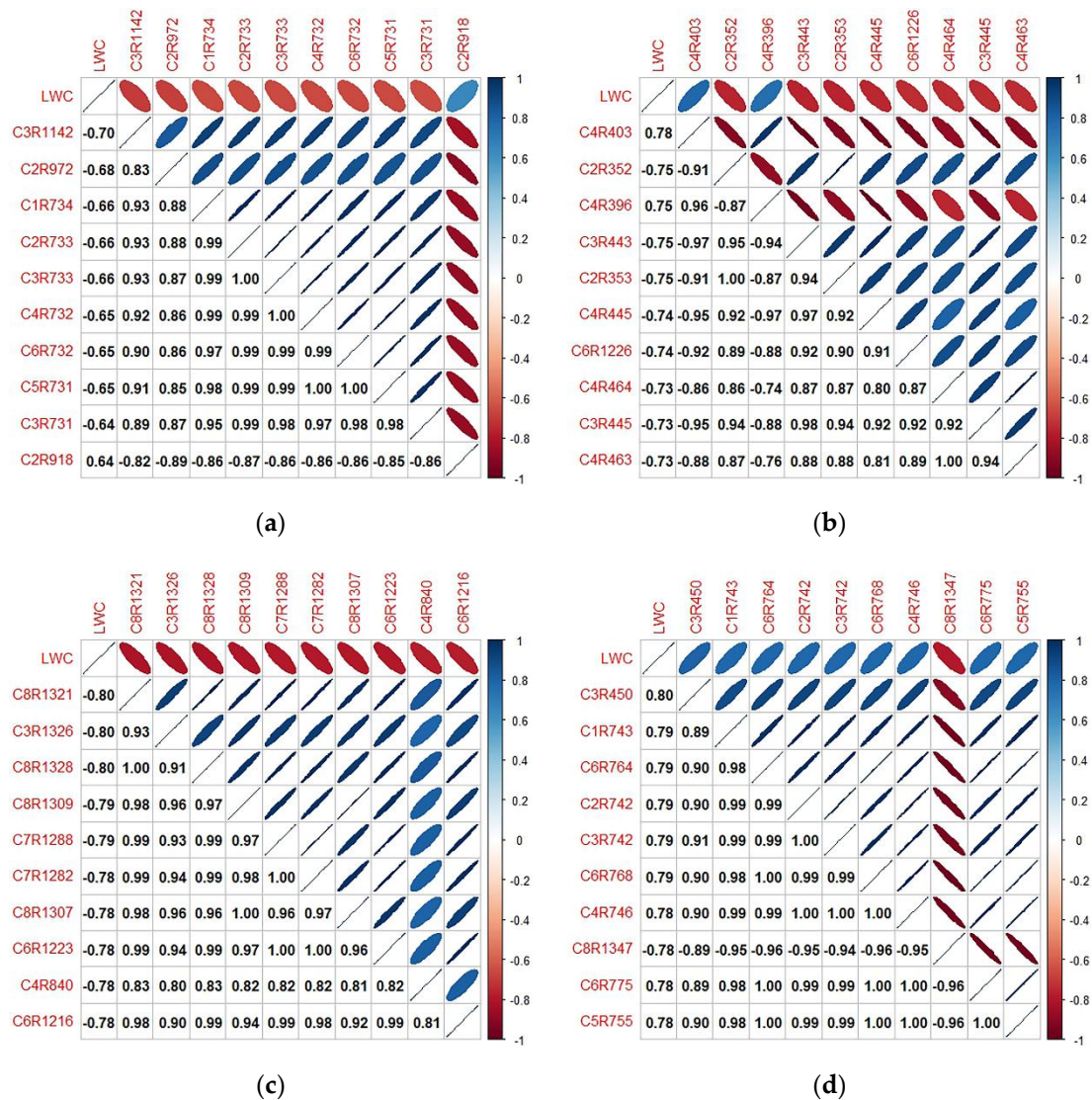


**Figure 6.** The relevance matrix of the selected wavelet coefficient with LWC in four growth periods. (a) Jointing period; (b) booting period; (c) flowering period; (d) filling period.

The following observations can be obtained from the analysis of Figures 5 and 6:

1. In the jointing period, the correlation between the wavelet coefficient and the LWC was analyzed. It could be seen from Figure 5a that the correlation between the wavelet coefficient and the LWC was stronger at first and then weakened as the decomposition scale increased from 1 to 10. Within the decomposition scale of 1 to 8, the maximum sizes of the wavelet coefficients and the LWC at each scale  $|\rho|$  were greater than 0.60. When the scale was 3, the  $|\rho|$  value reached the maximum of 0.70 at a wavelength of 1142 nm. Then, the 10 wavelet coefficients with a strong correlation with LWC were chosen as the independent variables, and their decomposition scales and bands were C3R1142, C2R972, C1R734, C2R733, C3R733, C4R732, C6R732, C5R731, C3R731, and C2R918, respectively. The correlation results are shown in Figure 6a.
2. In the booting period, the correlation between the wavelet coefficient and the LWC was analyzed. According to Figure 5b, the correlation between the wavelet coefficient and the LWC first became stronger and then weakened as the decomposition scale increased from 1 to 10. The maximum values of  $|\rho|$  between the wavelet coefficient and the LWC within the decomposition scale of 1 to 8 were greater than 0.71. When the scale was 4, the  $|\rho|$  was up to 0.78 at 403 nm. The 10 wavelet coefficients with a

strong correlation with LWC were chosen as the independent variables of the model, and their decomposition scales and bands were C4R403, C2R352, C4R396, C3R443, C2R353, C4R445, C6R1226, C4R464, C3R445, and C4R463, respectively. The correlation results are shown in Figure 6b.

3. In the flowering period, the correlation between the wavelet coefficient and the LWC was analyzed. It could be observed from Figure 5c that the correlation between the wavelet coefficient and the LWC was first stronger and then weakened as the decomposition scale increased from 1 to 10. Within the decomposition scale of 1 to 8, the maximum sizes of the wavelet coefficients and LWC at each scale  $|\rho|$  were greater than 0.70. When the scale was 8, the  $|\rho|$  reached the maximum of 0.80 at the wavelength of 1321 nm. Then, the 10 wavelet coefficients with a strong correlation with LWC were selected as the independent variables of the model, and their decomposition scales and bands were C8R1321, C3R1326, C8R1328, C8R1309, C7R1288, C7R1282, C8R1307, C6R1223, C4R840, and C6R1216, respectively. The correlation results are shown in Figure 6c.
4. In the filling period, the correlation between the wavelet coefficient and the LWC was analyzed. According to Figure 5d, the correlation between the wavelet coefficient and the LWC was stronger at first and then weakened as the decomposition scale increased from 1 to 10. The maximum values of  $|\rho|$  between the wavelet coefficient and LWC at the decomposition scale within 1 to 8 were greater than 0.77. When the scale was 3, the  $|\rho|$  was up to 0.80 at a wavelength of 450 nm. Then, the 10 wavelet coefficients with a strong correlation with LWC were selected as the independent variables of the model, and their decomposition scales and bands were C3R450, C1R743, C6R764, C2R742, C3R742, C6R768, C4R746, C8R1347, C6R775, and C5R755, respectively. The correlation results are shown in Figure 6d.

### 3.3.2. Construction and Analysis of LWC Estimation Model

In each growth period, the 10 wavelet coefficients screened were taken as independent variables and LWC as dependent variables. Then, 75% of the specimen data were randomly selected to build LWC estimation models for different growth periods of wheat by using three methods, namely, GPR, CART, and ANN. The remaining 25% of the specimen data were used to verify the accuracy of the model. The results are presented in Table 3.

**Table 3.** The LWC estimation results obtained by adopting wavelet coefficients combined with GPR, CART, and ANN for different growth periods.

Growth Periods	Method	Modeling Accuracy			Verification Accuracy		
		R <sup>2</sup>	RMSE (%)	nRMSE (%)	R <sup>2</sup>	RMSE (%)	nRMSE (%)
Jointing period	GPR	0.71 **	1.13	1.49	0.74 **	1.02	1.35
	CART	0.61 **	1.12	1.47	0.61 **	1.08	1.44
	ANN	0.72 **	0.86	1.13	0.76 **	0.98	1.28
Booting period	GPR	0.78 **	1.00	1.32	0.83 **	0.93	1.23
	CART	0.70 **	1.02	1.34	0.74 **	1.40	1.86
	ANN	0.70 **	1.00	1.32	0.73 **	0.96	1.26
Flowering period	GPR	0.88 **	1.11	1.51	0.88 **	1.66	2.26
	CART	0.75 **	1.09	1.48	0.77 **	1.87	2.52
	ANN	0.91 **	0.71	0.97	0.89 **	0.85	1.16
Filling period	GPR	0.84 **	4.67	7.55	0.85 **	4.25	6.86
	CART	0.74 **	4.93	8.11	0.77 **	7.61	12.92
	ANN	0.85 **	3.57	5.84	0.86 **	3.27	5.27

\*\* indicates  $p \leq 0.01$ .

The following observations are obtained from Table 3:

1. In the jointing period, the modeling accuracy of the ANN model was  $R^2 = 0.72$ , RMSE = 0.86%, and nRMSE = 1.13%, and the validation accuracy was  $R^2 = 0.76$ , RMSE = 0.98%, and nRMSE = 1.28%. Compared with the GPR model and the CART model, the modeling and validation  $R^2$  of the ANN increased by 0.10 and 0.13, and 0.11 and 0.15, and the RMSE decreased by 0.27% and 0.04%, 0.26% and 0.10%, and the nRMSE decreased by 0.36% and 0.07%, and 0.34% and 0.16%, respectively. The ANN model achieved higher modeling and verification accuracy than the other two models. Through a comprehensive analysis, it was found that the ANN model achieved a better estimation effect in the jointing period.
2. In the booting period, the modeling accuracy of the GPR model was  $R^2 = 0.78$ , RMSE = 1.00%, and nRMSE = 1.32%, and the validation accuracy was  $R^2 = 0.83$ , RMSE = 0.93%, and nRMSE = 1.23%. Compared with the CART model and the ANN model, the modeling and validation  $R^2$  of the GPR increased by 0.08 and 0.08, and 0.09 and 0.10, and the RMSE decreased by 0.02% and 0.47%, and 0.00% and 0.03%, and the nRMSE decreased by 0.02% and 0.63%, and 0.00% and 0.03%, respectively. The modeling and validation accuracy of the GPR model was higher than that of the other two models. A comprehensive analysis indicated that the GPR model achieved a better estimation effect in the booting period.
3. In the flowering period, the modeling accuracy of the ANN model was  $R^2 = 0.91$ , RMSE = 0.71%, nRMSE = 0.97%, and the validation accuracy was  $R^2 = 0.89$ , RMSE = 0.85%, and nRMSE = 1.16%. Compared with the GPR model and the CART model, the modeling and validation  $R^2$  of the ANN increased by 0.03 and 0.01, and 0.16 and 0.12, and the RMSE decreased by 0.40% and 0.81%, and 0.38% and 1.02%, and the nRMSE decreased by 0.54% and 1.10%, and 0.51% and 1.36%, respectively. The modeling and validation accuracy of the ANN model was higher than that of the other two models. Through a comprehensive analysis, it was found that the ANN model had the highest estimation accuracy in the flowering period.
4. In the filling period, the modeling accuracy of the ANN model was  $R^2 = 0.85$ , RMSE = 3.57%, and nRMSE = 5.84%, and the validation accuracy was  $R^2 = 0.86$ , RMSE = 3.27%, and nRMSE = 5.27%. Compared with the GPR model and the CART model, the modeling and validation  $R^2$  of the ANN increased by 0.01 and 0.01, and 0.11 and 0.09, and the RMSE decreased by 1.10% and 0.98%, and 1.36% and 4.34%, and the nRMSE decreased by 1.71% and 1.59%, and 2.27% and 7.65%, respectively. The modeling and validation accuracy of the ANN model was higher than that of the other two models. A comprehensive analysis indicated that the ANN model achieved a better estimation effect in the filling period.

When using wavelet coefficients combined with the GPR, CART, and ANN methods to estimate LWC in different growth periods, the ANN model at the jointing, flowering, and filling periods achieved the highest estimation accuracy, and the GPR model obtained the best estimation effect in the booting period.

### 3.4. Estimation of Wheat LWC Based on Mixed Variables

In the four growth periods, the differential spectrum and wavelet coefficients screened previously were taken as model variables, and three methods of GPR, CART, and ANN were used to estimate the LWC. Table 4 shows the estimated results of LWC.

The following observations are obtained from Table 4:

1. In the jointing period, the modeling accuracy of the GPR model was  $R^2 = 0.77$ , RMSE = 1.04%, and nRMSE = 1.37%, and the validation accuracy was  $R^2 = 0.77$ , RMSE = 0.93%, and nRMSE = 1.22%. Compared with the CART model and the ANN model, the modeling and validation  $R^2$  of the GPR increased by 0.15 and 0.11, and 0.17 and 0.10, and the RMSE decreased by 0.06% and 0.29%, and 0.03% and 0.37%, and the nRMSE decreased by 0.08% and 0.40%, and 0.04% and 0.49%, respectively. The GPR model achieved higher modeling and verification accuracy than the other

- two models. Through a comprehensive analysis, it was found that the GPR model achieved a better estimation effect in the jointing period.
- In the booting period, the modeling accuracy of the GPR model was  $R^2 = 0.83$ , RMSE = 0.86%, and nRMSE = 1.12%, and the validation accuracy was  $R^2 = 0.81$ , RMSE = 0.72%, and nRMSE = 0.94%. Compared with the CART model and the ANN model, the modeling and validation  $R^2$  of the GPR increased by 0.08 and 0.06, and 0.10 and 0.07, and the RMSE decreased by 0.06% and 0.46%, and 0.07% and 0.19%, and the nRMSE decreased by 0.09% and 0.61%, and 0.09% and 0.25%, respectively. The modeling and validation accuracy of the GPR model was higher than that of the other two models. A comprehensive analysis indicated that the GPR model achieved a better estimation effect in the booting period.
  - In the flowering period, the modeling accuracy of the ANN model was  $R^2 = 0.92$ , RMSE = 0.64%, nRMSE = 0.87%, and the validation accuracy was  $R^2 = 0.91$ , RMSE = 0.82%, and nRMSE = 1.12%. Compared with the GPR model and the CART model, the modeling and validation  $R^2$  of the ANN increased by 0.02 and 0.02, and 0.09 and 0.05, and the RMSE decreased by 0.31% and 0.18%, and 0.30% and 0.68%, and the nRMSE decreased by 0.43% and 0.25%, and 0.41% and 0.90%, respectively. The modeling and validation accuracy of the ANN model was higher than that of the other two models. Through a comprehensive analysis, it was found that the ANN model had the highest estimation accuracy in the flowering period.
  - In the filling period, the modeling accuracy of the ANN model was  $R^2 = 0.86$ , RMSE = 3.14%, and nRMSE = 5.09%, and the validation accuracy was  $R^2 = 0.83$ , RMSE = 6.01%, and nRMSE = 9.57%. Compared with the GPR model and the CART model, the modeling and validation  $R^2$  of the ANN increased by 0.01 and 0.04, and 0.10 and 0.08, and the RMSE decreased by 0.94% and 0.43%, and 1.68% and 1.84%, and the nRMSE decreased by 1.46% and 0.68%, and 2.81% and 4.14%, respectively. The modeling and validation accuracy of the ANN model was higher than that of the other two models. A comprehensive analysis indicated that the ANN model achieved a better estimation effect in the filling period.

**Table 4.** The LWC estimation results obtained by using differential spectrum and wavelet coefficients combined with GPR, CART, and ANN for different growth periods.

Growth Periods	Method	Modeling Accuracy			Verification Accuracy		
		$R^2$	RMSE (%)	nRMSE (%)	$R^2$	RMSE (%)	nRMSE (%)
Jointing period	GPR	0.77 **	1.04	1.37	0.77 **	0.93	1.22
	CART	0.62 **	1.10	1.45	0.66 **	1.22	1.62
	ANN	0.60 **	1.07	1.41	0.67 **	1.30	1.71
Booting period	GPR	0.75 **	0.92	1.21	0.75 **	1.18	1.55
	CART	0.83 **	0.86	1.12	0.81 **	0.72	0.94
	ANN	0.73 **	0.93	1.21	0.74 **	0.91	1.19
Flowering period	GPR	0.90 **	0.95	1.30	0.89 **	1.00	1.37
	CART	0.81 **	0.94	1.28	0.86 **	1.50	2.02
	ANN	0.92 **	0.64	0.87	0.91 **	0.82	1.12
Filling period	GPR	0.85 **	4.08	6.55	0.79 **	6.44	10.25
	CART	0.76 **	4.82	7.90	0.75 **	7.85	13.71
	ANN	0.86 **	3.14	5.09	0.83 **	6.01	9.57

\*\* indicates  $p \leq 0.01$ .

When using mixed variables combined with GPR, CART, and ANN methods to estimate LWC in different growth periods, the GPR model obtained the best estimation ability in the jointing and booting periods, the ANN model at the flowering and filling periods achieved the highest estimation accuracy.

#### 4. Discussion

Analyzing the LWC estimation results of wheat in different periods, it could be seen that the overall LWC estimation effect was very good, the  $R^2$  of modeling and verification reached 0.92 and 0.91, and the mean value reached 0.77 and 0.78, respectively. This is because the hyperspectral data have a high resolution and strong band continuity, which can correctly mirror the spectral characteristics and differences of crops and correctly obtain some agricultural information. Thus, the method is suitable for monitoring the physiological and biochemical parameters of crops. The difficulty of estimating crop LWC by adopting hyperspectral data lies in the influence of external interference factors when collecting data, which leads to noise in spectral data and affects the extraction of susceptible information [35]. After processing with fractional differential and continuous wavelet transform, the influence of noise can be eliminated, and the sensitive messages in spectral data can be deeply mined, further improving the estimation accuracy of crop LWC. This is consistent with the research results in the literature [14,36,37].

The spectral characteristics of crops are closely related to their growth periods, health status, and external environment, and the spectral curves of crops in different growth periods will show varying change characteristics, so the estimation models constructed with data of one growth period generally have poor universality [38,39]. Therefore, this paper collected the experimental data from four key periods of jointing, booting, flowering, and filling for modeling. By analyzing the LWC estimation results of the four growth periods, it could be seen that in the four periods, the estimation ability of the jointing period was relatively poor, and the mean value of  $R^2$  in modeling and verification was only 0.66 and 0.70, respectively. In the booting period, the mean values of  $R^2$  were 0.75 and 0.77, respectively, which was slightly better than that in the jointing period. In the flowering period, the average values of  $R^2$  for modeling and verification were 0.86 and 0.87, and those in the filling period were 0.81 and 0.81, respectively. It showed that the LWC estimation accuracy in the flowering period was higher than that in the filling period. This may be because the LWC of wheat in the flowering period gradually decreases and changes greatly, and the sensitivity of LWC to hyperspectral data is relatively strong. This is consistent with the research results in the literature [20,40].

In the four growth periods, a comprehensive analysis of the LWC estimation results of using differential spectrum and wavelet coefficient combined with GPR, CART, and ANN models indicated that compared with the differential spectrum and wavelet coefficient, the LWC estimation using combined mixed variables contributed to better results. The maximum  $R^2$  of modeling and testing could reach 0.92 and 0.91, and the average value could reach 0.78 and 0.79. This is because fractional differential and wavelet transform can eliminate the influence of noise in spectral information, improve the sensitivity of LWC to spectral data, and further enhance the stability and robustness of the model. This is compatible with the study results in the literature [13,16,41].

By comparing and analyzing the LWC estimation results based on different methods in different growth periods, it was found that in the jointing period, the mixed variables combined with the ANN model achieved a better effect in estimating LWC, and the  $R^2$  of modeling and testing was 0.77 and 0.77, respectively. In the booting period, the mixed variables combined with the GPR model performed better in estimating LWC, and the  $R^2$  of modeling and testing was 0.83 and 0.81, respectively. In the flowering period, using the mixed variables combined with the ANN model to estimate LWC obtained the highest accuracy, the  $R^2$  of modeling and testing was 0.92 and 0.91, respectively. In the filling period, using the wavelet coefficient combined with the ANN model to estimate LWC contributed to high accuracy, and the  $R^2$  of modeling and testing was 0.85 and 0.86, respectively.

This work proposed to transform and process the hyperspectral data by adopting fractional order differential and continuous wavelet transform, which can effectively abate the noise impact in spectral data and improve the estimation effect of wheat LWC. The accurate monitoring of LWC can effectively diagnose wheat water status, provide basic information for wheat growth monitoring and drought monitoring, and is of great signifi-

cance for achieving a stable and high yield of wheat [24]. The research results can provide a reference for LWC based on remote sensing technology. In addition, fractional differential and continuous wavelet transform can also be applied to other crop phenotypic traits (such as biomass, chlorophyll, and nitrogen content).

## 5. Conclusions

Based on two data processing methods of fractional order differential and continuous wavelet transform, this work processed the original hyperspectral data of winter wheat in four periods. Then, the original hyperspectral data, differential spectrum, and wavelet coefficients were analyzed, and the analysis results were compared to obtain 10 differential spectra and 10 wavelet coefficients that were more closely related to LWC. Subsequently, the LWC estimation models for different growth periods of winter wheat were built by using GPR, CART, and ANN methods. Through analyzing the modeling and verification results of the model, the optimal LWC estimation model for each growth period and the growth period with the highest precision of LWC estimation were determined, providing new ideas for estimating crop LWC. Although this work has obtained some research results, several defects need to be addressed.

When a machine learning algorithm is used for modeling, a large number of samples are required. The work used a small amount of sample data, resulting in overfitting, which reduced the stability of the model. In future studies, the number of samples, sample years, wheat varieties, etc. can be increased to verify the model, thus further improving the stability and universality of the model. Meanwhile, because of the constriction of experimental factors, the work used data of a piece of farmland, without considering the influence of different areas on the experimental data. In the future, it is necessary to take experimental data from multiple areas and use more sample experimental data to train models, thus achieving better estimation effects and stronger robustness.

**Author Contributions:** Conceptualization, C.L.; data curation, Y.L. (Yanghua Liu); methodology, Z.X.; software, Z.X.; validation, Z.X.; formal analysis, X.M. and X.L.; investigation, X.W. and Y.L. (Yafeng Li); resources, C.Z.; writing—original draft preparation, Z.X.; writing—review and editing, C.L.; visualization, L.R. and C.Y.; supervision, Y.J.; project administration, C.L.; funding acquisition, C.L. All authors have read and agreed to the published version of the manuscript.

**Funding:** This research was supported by the National Natural Science Foundation of China (41871333), the National Innovation and Entrepreneurship Training Program for College Students (202210460019), and the Key Project of Science and Technology of the Henan Province (222102110038).

**Data Availability Statement:** Not applicable.

**Acknowledgments:** We are grateful to the anonymous reviewers for their comments and recommendations.

**Conflicts of Interest:** The authors declare no conflict of interest.

## References

1. Guo, J.M.; Gao, Y.F.; Li, S.T.; Pema, R.; Wang, Y.Y.; Zhang, Y.J.; Liu, R.H. Estimation model of leaf water content of winter wheat based on multi-angle hyperspectral remote sensing. *J. Anhui Agric. Univ.* **2019**, *46*, 124–132. (In Chinese)
2. Hassanli, A.M.; Ahmadi-rad, S.; Beecham, S. Evaluation of the influence of irrigation methods and water quality on sugar beet yield and water use efficiency. *Agric. Water Manag.* **2010**, *97*, 357–362. [[CrossRef](#)]
3. Zhang, W.; Wang, X.M.; Pan, Q.M.; Xie, J.Z.; Zhang, J.S.; Meng, P. Spectral reflectance characteristics of *Phyllostachys violascens* canopy leaves in response to water change. *For. Res.* **2019**, *32*, 73–79. (In Chinese)
4. Liu, S.G.; Hu, Z.Q.; Han, J.Z.; Li, Y.Y.; Zhou, T. Predicting grain yield and protein content of winter wheat at different growth stages by hyperspectral data integrated with growth monitor index. *Comput. Electron. Agric.* **2022**, *200*, 107235. [[CrossRef](#)]
5. Yue, J.B.; Feng, H.K.; Yang, G.J.; Li, Z.H. A comparison of regression techniques for estimation of above-ground winter wheat biomass using near-surface spectroscopy. *Remote Sens.* **2018**, *10*, 66. [[CrossRef](#)]
6. Wang, F.M.; Yi, Q.X.; Hu, J.H.; Xie, L.L.; Yao, X.P.; Xu, T.Y.; Zheng, J.Y. Combining spectral and textural information in UAV hyperspectral images to estimate rice grain yield. *Int. J. Appl. Earth Obs. Geoinf.* **2021**, *102*, 102397. [[CrossRef](#)]

7. Song, X.; Xu, D.Y.; Huang, S.M.; Huang, C.C.; Zhang, S.Q.; Guo, D.D.; Zhang, K.K.; Yue, K. Nitrogen content inversion of wheat canopy leaf based on ground spectral reflectance data. *Chin. J. Appl. Ecol.* **2020**, *31*, 1636–1644. (In Chinese)
8. Yang, F.Q.; Feng, H.K.; Li, Z.H.; Gao, L.; Yang, G.J.; Dai, H.Y. Hyperspectral estimation of leaf area index for winter wheat based on Akaike's information criterion. *Trans. Chin. Soc. Agric. Eng.* **2016**, *32*, 163–168. (In Chinese)
9. Pan, Q.M.; Zhang, J.S.; Zhang, J.P.; Meng, P.; Wang, G.B.; Yang, H.G.; Wang, X.M.; Yuan, W.W.; Zhou, Y. Analysis of correlation and differences between leaf moisture and hyperspectral reflectance among different walnut varieties. *For. Res.* **2019**, *32*, 1–6. (In Chinese)
10. Li, Y.M.; Zhang, X.J. Remote sensing monitoring of leaf water content in *Lycium barbarum* based on spectral index. *Geogr. Geo-Inf. Sci.* **2019**, *35*, 16–21. (In Chinese)
11. Seelig, H.D.; Hoehn, A.; Stodieck, L.S.; Klaus, D.M.; Adams III, W.W.; Emery, W.J. The assessment of leaf water content using leaf reflectance ratios in the visible, near-, and short-wave-infrared. *Int. J. Remote Sens.* **2008**, *29*, 3701–3713. [\[CrossRef\]](#)
12. Kong, W.P.; Huang, W.J.; Ma, L.L.; Tang, L.L.; Li, C.R.; Zhou, X.F.; Casa, R. Estimating vertical distribution of leaf water content within wheat canopies after head emergence. *Remote Sens.* **2021**, *13*, 4125. [\[CrossRef\]](#)
13. Li, C.C.; Shi, J.J.; Ma, C.Y.; Cui, Y.Q.; Wang, Y.L.; Li, Y.C. Estimation of chlorophyll content in winter wheat based on wavelet transform and fractional differential. *Trans. Chin. Soc. Agric. Mach.* **2021**, *52*, 172–182. (In Chinese)
14. Zhang, Z.T.; Lao, C.C.; Wang, H.F.; Arnon, K.; Chen, J.Y.; Li, Y. Estimation of desert soil organic matter through hyperspectral based on fractional-order derivatives and SVM-DA-RF. *Trans. Chin. Soc. Agric. Mach.* **2020**, *51*, 156–167. (In Chinese)
15. Wumuti, A.; Maimaiti, S.; Ma, C.Y. Hyperspectral estimation of wheat leaf water content using fractional differentials and successive projection algorithm-back propagation neural network. *Laser Optoelectron. Prog.* **2019**, *56*, 251–259. (In Chinese)
16. Ebrahimi, H.; Rajaei, T. Simulation of groundwater level variations using wavelet combined with neural network, linear regression and support vector machine. *Glob. Planet. Change.* **2017**, *148*, 181–191. [\[CrossRef\]](#)
17. Blackburn, G.A.; Ferwerda, J.G. Retrieval of chlorophyll concentration from leaf reflectance spectra using wavelet analysis. *Remote Sens. Environ.* **2008**, *112*, 1614–1632. [\[CrossRef\]](#)
18. Lin, D.; Li, G.; Zhu, Y.D.; Liu, H.; Li, L.; Fahad, S.; Zhang, X.; Wei, C.; Jiao, Q. Predicting copper content in chicory leaves using hyperspectral data with continuous wavelet transforms and partial least squares. *Comput. Electron. Agric.* **2021**, *187*, 106293. [\[CrossRef\]](#)
19. Tan, X.M.; Wang, Z.L.; Zhang, J.W.; Yang, F.; Yang, W.Y. Estimation of maize canopy chlorophyll density under drought stress based on continuous wavelet transform. *Agric. Res. Arid. Areas* **2021**, *39*, 155–161. (In Chinese)
20. Wang, Y.C.; Zhang, X.Y.; Jin, Y.T.; Gu, X.H.; Feng, H.; Wang, C. Quantitative retrieval of water content in winter wheat leaves based on continuous wavelet transform. *J. Triticeae Crops* **2020**, *40*, 503–509. (In Chinese)
21. Yansenjiang, K.; Yang, S.T.; Nigela, T.; Zhang, F. Hyperspectral estimation of soil electrical conductivity based on fractional order differentially optimised spectral indices. *Acta Ecol. Sin.* **2019**, *39*, 7237–7248. (In Chinese)
22. Zhang, Y.K.; Luo, B.; Pan, D.Y.; Song, P.; Lu, W.C.; Wang, C.; Zhao, C.J. Estimation of canopy nitrogen content of soybean crops based on fractional differential algorithm. *Spectrosc. Spectr. Anal.* **2018**, *38*, 3221–3230. (In Chinese)
23. Jin, X.L.; Yang, G.J.; Xu, X.G.; Yang, H.; Feng, H.; Li, Z.; Shen, J.; Lan, Y.; Zhao, C. Combined multi-temporal optical and radar parameters for estimating LAI and biomass in winter wheat using HJ and RADARSAR-2 data. *Remote Sens.* **2015**, *7*, 13251–13272. [\[CrossRef\]](#)
24. Li, C.; Wang, Y.C.; Li, X.Q.; Yang, X.F.; Gu, X.H. Quantitative Inversion of Water Content of Plant Components in Winter Wheat Based on Wavelet Technology. *Trans. Chin. Soc. Agric. Mach.* **2021**, *52*, 193–201. (In Chinese)
25. Peng, Y.S.; Chen, S.S.; Chen, J.Y.; Zhao, J.; Wang, C.Y.; Guan, Y.L. Estimation model of chlorophyll a concentration based on continuous wavelet coefficients. *Laser Optoelectron. Prog.* **2021**, *58*, 431–439. (In Chinese)
26. Miao, M.K.; Wang, B.S.; Li, C.C.; Long, H.L.; Yang, G.J.; Feng, H.K.; Zhai, L.T.; Liu, M.X.; Wu, Z.C. Remote sensing estimation of the maximum net photosynthetic rate of winter wheat leaves based on continuous wavelet transform. *Jiangsu J. Agric. Sci.* **2020**, *36*, 544–552. (In Chinese)
27. Zhang, T.; Yu, L.; Yi, J.; Nie, Y.; Zhou, Y. Determination of soil organic matter content based on hyperspectral wavelet energy features. *Spectrosc. Spectr. Anal.* **2019**, *39*, 3217–3222. (In Chinese)
28. Wang, R.; Wan, D.S. Feature extraction method of hydrological time series based on support vector regression and gaussian process regression. *Sci. Technol. Eng.* **2021**, *21*, 10774–10779. (In Chinese)
29. Williams, C.K.; Rasmussen, C.E. *Gaussian Processes for Machine Learning*; MIT Press Cambridge: Cambridge, MA, USA, 2006.
30. Wang, H.; Zhang, W.J.; Liu, J.; Chen, L.F.; Li, Z.N. Flight delay prediction model based on CART algorithm. *J. Civ. Aviat. Univ. China* **2022**, *40*, 35–40. (In Chinese)
31. Khoshnevisan, B.; Rafiee, S.; Omid, M.; Mousazadeh, H.; Sefeedpari, P. Prognostication of environmental indices in potato production using artificial neural networks. *J. Clean. Prod.* **2013**, *52*, 402–409. [\[CrossRef\]](#)
32. Li, C.C.; Wang, Y.L.; Ma, C.Y.; Chen, W.N.; Li, Y.C.; Li, J.B.; Ding, F.; Xiao, Z. Improvement of Wheat Grain Yield Prediction Model Performance Based on Stacking Technique. *Appl. Sci.* **2021**, *11*, 12164. [\[CrossRef\]](#)
33. Xu, X.B.; Nie, C.W.; Jin, X.L.; Li, Z.H.; Zhu, H.C.; Xu, H.G.; Wang, J.W.; Zhao, Y.; Feng, H.K. A comprehensive yield evaluation indicator based on an improved fuzzy comprehensive evaluation method and hyperspectral data. *Field Crops Res.* **2021**, *270*, 108204. [\[CrossRef\]](#)

34. Yue, J.B.; Yang, G.J.; Feng, H.K. Comparative of remote sensing estimation models of winter wheat biomass based on random forest algorithm. *Trans. Chin. Soc. Agric. Eng.* **2016**, *32*, 175–182. (In Chinese)
35. Li, C.C.; Li, Y.C.; Wang, Y.L.; Ma, C.Y.; Chen, W.N.; Ding, F. Winter wheat biomass estimation based on wavelet energy coefficient and leaf area index. *Trans. Chin. Soc. Agric. Mach.* **2021**, *52*, 191–200. (In Chinese)
36. Fang, S.H.; Le, Y.; Liang, Q. Retrieval of chlorophyll content using continuous wavelet analysis across a range of vegetation species. *Geomat. Inf. Science Wuhan Univ.* **2015**, *40*, 296–302. (In Chinese)
37. Yao, S.N.; Jiang, J.B.; Shi, X.X.; Wang, W.J.; Meng, H. Hyperspectral estimation of canopy chlorophyll content in soybean under natural gas micro leakage stress. *Geogr. Geo-Inf. Sci.* **2019**, *35*, 22–27. (In Chinese)
38. Liu, B.F. Monitoring Models of Physiological and Ecological Parameters of Summer Maize Based on Hyperspectral Remote Sensing at Different Growth Stages. Doctor's Thesis, Northwest A&F University, Xianyang, China, 2016. (In Chinese).
39. Sun, B.Y.; Chang, Q.R.; Liu, M.Y. Inversion chlorophyll mass fraction in winter wheat canopy by hyperspectral reflectance. *Acta Agric. Boreali-Occident. Sin.* **2017**, *26*, 552–559. (In Chinese)
40. Li, K.; Chang, Q.R.; Chen, Q.; Chen, X.K.; Mo, H.Y.; Zhang, Y.D.; Zheng, Z.K. Estimation of water content in canopy leaf of winter wheat based on continuous wavelet transform coupled CARS algorithm. *J. Triticeae Crops* **2022**, *42*, 1–8. (In Chinese)
41. Cheng, T.; Rivard, B.; Sanchez-Azofeifa, A.G.; Féret, J.B.; Jacquemoud, S.; Ustin, S.L. Predicting leaf gravimetric water content from foliar reflectance across a range of plant species using continuous wavelet analysis. *J. Plant Physiol.* **2012**, *169*, 1134–1142. [[CrossRef](#)]

**Disclaimer/Publisher's Note:** The statements, opinions and data contained in all publications are solely those of the individual author(s) and contributor(s) and not of MDPI and/or the editor(s). MDPI and/or the editor(s) disclaim responsibility for any injury to people or property resulting from any ideas, methods, instructions or products referred to in the content.